

## Effect of Nb on Microstructural Evolution and Mechanical Properties of Hot-Rolled Quenching and Partitioning Steels Containing Bainite

Chai, Zhisong; Hu, Jun; Wang, Chenchong; Wang, Lingyu; Sun, Weihua; van der Zwaag, Sybrand; Xu, Wei

**DOI**

[10.1002/srin.202100247](https://doi.org/10.1002/srin.202100247)

**Publication date**

2021

**Document Version**

Final published version

**Published in**

Steel Research International

**Citation (APA)**

Chai, Z., Hu, J., Wang, C., Wang, L., Sun, W., van der Zwaag, S., & Xu, W. (2021). Effect of Nb on Microstructural Evolution and Mechanical Properties of Hot-Rolled Quenching and Partitioning Steels Containing Bainite. *Steel Research International*, 92(12), 10. Article 2100247. <https://doi.org/10.1002/srin.202100247>

**Important note**

To cite this publication, please use the final published version (if applicable). Please check the document version above.

**Copyright**

Other than for strictly personal use, it is not permitted to download, forward or distribute the text or part of it, without the consent of the author(s) and/or copyright holder(s), unless the work is under an open content license such as Creative Commons.

**Takedown policy**

Please contact us and provide details if you believe this document breaches copyrights. We will remove access to the work immediately and investigate your claim.

***Green Open Access added to TU Delft Institutional Repository***

***'You share, we take care!' - Taverne project***

**<https://www.openaccess.nl/en/you-share-we-take-care>**

Otherwise as indicated in the copyright section: the publisher is the copyright holder of this work and the author uses the Dutch legislation to make this work public.

# Effect of Nb on Microstructural Evolution and Mechanical Properties of Hot-Rolled Quenching and Partitioning Steels Containing Bainite

Zhisong Chai, Jun Hu, Chenchong Wang, Lingyu Wang, Weihua Sun, Sybrand van der Zwaag, and Wei Xu\*

Herein, the effect of Nb content on the phase transformation kinetics, microstructure, and mechanical properties of hot-rolled quenching and partitioning (Q&P) steel is investigated. The characteristics of three C–Mn–Si–Ti steels (0.18C, 2.0Si, 2.6Mn, and 0.015Ti) containing 0, 0.027, or 0.061 wt% Nb are compared. Results reveal that grain boundary pinning by precipitates and Nb solute drag effects refine the austenite grain size during the hot-rolling process; the microstructural refinement is carried over to the final microstructure subjected to the Q&P treatment. The remaining supersaturated Nb suppresses the bainite formation and decreases the final bainite fraction formed in the Q&P process. The microstructural evolution leads to an increase in the ultimate tensile strength (UTS) of the steel containing 0.027 wt% Nb from 1169 to 1228 MPa, while keeping the total elongation at 18%. When the Nb content is increased to 0.061 wt%, the UTS of the steel increases to 1313 MPa, but the elongation at break drops to 16%. The effect is due to the carbon consumption by the Nb precipitates, which causes a decrease in the stability of the retained austenite and reduces the strain hardening at high strain levels.

attention from the global steel industry because of their combination of high strength and high ductility. To obtain the highest-grade Q&P steels, many research efforts have been directed at improving its combination of mechanical properties through additional microstructural control<sup>[6–9]</sup> and optimization of the chemical composition.<sup>[10–13]</sup>

Q&P steels belong to the family of low-alloy multiphase high-strength steel, in which a certain amount of retained austenite (RA) transforms to martensite upon elastic-plastic deformation at room temperature thereby exerting the so-called transformation-induced plasticity (TRIP) effect; The transformation leads to the enhancement of the strain hardening and hence to a more desirable combination of high strength and high ductility. The main concept behind the Q&P process is that carbon in the supersaturated martensite dif-

fuses into the parent (yet unstable) austenite through the martensite/austenite interface during moderate-temperature tempering after controlled quenching to a temperature in the martensite transformation region. The carbon enrichment stabilizes the RA and ensures its (partial) retention upon final cooling to room temperature. The Q&P process in itself is relatively simple, can be expanded into different process variants and can be applied to a relatively wide range of steel chemistries.<sup>[3]</sup> While sticking to the key ingredients of the Q&P treatment, extensive studies have been conducted to tune the volume fraction of RA, its morphology, its carbon content as well as the matrix microstructure either consisting of martensite or martensite and ferrite. Excellent combinations of mechanical properties have been achieved.<sup>[14–17]</sup> The introduction of bainite into Q&P steels can lead to even better strength and plasticity. Zhao et al.<sup>[7]</sup> reported that bainite formation in the partitioning stage below the martensite start ( $M_s$ ) temperature can contribute to the enhancement of the yield strength (YS) of Q&P steels. In addition, Peng et al.<sup>[8]</sup> found that the bainite formation is an effective method to stabilize austenite in the partitioning process, whereas the appearance of fresh martensite can be prevented in the final quenching stage, resulting in an improved elongation at break; Similar results have been reported by Kong et al.<sup>[18]</sup> However, the research on the microstructural design of Q&P steels to achieve outstanding mechanical properties is still not finished.


## 1. Introduction

For some decades, the research and development of automobile steel has focused on the design of materials with high strength and plasticity to decrease the weight of vehicles, while improving the safety of automobiles.<sup>[1–4]</sup> Quenching and partitioning (Q&P) steels<sup>[5]</sup> are one of the most promising candidates among the third-generation automobile steels, and have attracted significant

Z. Chai, J. Hu, C. Wang, L. Wang, W. Xu  
State Key Laboratory of Rolling and Automation  
Northeastern University  
Shenyang 110819, China  
E-mail: xuwei@ral.neu.edu.cn

W. Sun  
Shandong Iron & Steel Group Rizhao Co., Ltd.  
Shandong 276805, China

S. van der Zwaag  
Novel Aerospace Materials group  
Delft University of Technology  
Kluyverweg 1, Delft 2629 HS, The Netherlands

 The ORCID identification number(s) for the author(s) of this article can be found under <https://doi.org/10.1002/srin.202100247>.

DOI: 10.1002/srin.202100247

To further improve the strength, ductility, work hardening, and other mechanical properties of Q&P steels, a conventional microalloying element such as Nb can be added.<sup>[19]</sup> Nb has the ability to improve the strength of construction steels without affecting its elongation because it controls the recrystallization process such that finer prior austenite grain size is obtained.<sup>[20,21]</sup> In addition, the formation of niobium carbo-nitride Nb (C, N) particles at lower process temperatures will lead to precipitation strengthening. Thus, Nb is favored by researchers in the field of Q&P steels as the most promising microalloying element. For instance, Zhong et al.<sup>[22]</sup> demonstrated that adding 0.05Nb to a 0.2C–1.5Mn–1.5Si–0.3Mo (wt%) steel can result in a better combination of strength and elongation given the appropriate Q&P process variant. According to Zhang et al.,<sup>[10]</sup> adding 0–0.025Nb to 0.2C–1.5Si–1.5Mn–0.15Al (wt%) steel is beneficial to increase the volume fraction of RA; but a high Nb content decreases the volume fraction of RA as a result of carbon scavenging in the Nb precipitation, leading to a decrease in ductility. Hence, several studies have shown that the addition of an optimal amount of Nb can result in the formation of a uniform microstructure with a small but stable RA fraction and therefore in a steel with an excellent combination of strength and elongation.

Although earlier studies have investigated the effects of Nb on RA stabilization, the effect of the Nb content on the microstructural evolution and properties of a bainitic Q&P steel is not so well documented. Therefore, in this study, the process route of water quenching after hot rolling followed by one-step partitioning is used to clarify the effect of Nb on the microstructural evolution, in particular, the bainitic transformation behavior, the mechanical stability of RA, and the mechanical properties. The base chemistry of the steel was selected to be 0.19C–2Si–2.60Mn–0.015Ti (all compositions in wt%), as this composition is well located in the generally preferred compositional domain for Q&P steels,<sup>[2]</sup> but this exact composition has not been studied yet.

## 2. Experimental Section

### 2.1. Materials

The compositions of the three types of Q&P steels used in this work are shown in Table 1. The steel specimens had a low hypo-eutectoid carbon content of 0.18 wt% and different Nb contents, viz., steel A without Nb, steel B with 0.027 wt% Nb, and steel C with 0.061 wt% Nb. All steels had 2.0 wt% Si (to suppress cementite formation) and 2.6 wt% Mn (to reduce the bainitic transformation temperature and  $M_s$  value). Thermo-Calc software was used to determine the starting and finishing temperatures of the crucial austenite formation,  $A_{e1}$  and  $A_{e3}$ , respectively. The starting temperature of the formation of martensite,

**Table 1.** Chemical compositions of the three experimental steels (wt%).

Steels	C	Si	Mn	Ti	Nb	Fe
A	0.175	2.00	2.59	0.015	0	Bal.
B	0.179	2.07	2.60	0.016	0.027	Bal.
C	0.180	2.07	2.60	0.014	0.061	Bal.

$M_s$  was calculated by JMatPro. The results showed that there is no significant difference in the key phase transformation temperatures, with values for  $A_{e3}$ ,  $A_{e1}$ , and  $M_s$  of approximately 840, 672, and 340 °C for all three steels.

### 2.2. Processing Route

A schematic of the hot rolling process and Q&P treatment is shown in Figure 1. The production of the experimental steel samples proceeded via a multistep process. Initially, 100 kg ingots were melted in a vacuum induction furnace, forged into billets ( $210 \times 120 \times 80 \text{ mm}^3$ ), and then heated in a furnace at 1200 °C for 2 h. Next, 3 mm-thick slabs were produced by hot rolling the ingots in seven passes between 1100 and 860 °C, followed by water quenching to room temperature. Subsequently, the water-quenched sheets were heated at a rate of  $10 \text{ °C s}^{-1}$  to the dual phase region at 820 °C where the sheets were held for 300 s, and then cooled at the rate of  $30 \text{ °C s}^{-1}$  to a quenching temperature of 300 °C, after which the sheets were immersed for 500 s in a salt bath kept at this temperature. The final process step involved water quenching to room temperature.

### 2.3. Microstructural Characterization

Microstructural characterization of the heat-treated steels was carried out by optical microscopy (OM) and scanning electron microscopy (SEM). For OM observations with a Leica DM 2500M optical microscope, mechanically polished samples were etched in a 2% nital solution to reveal the microstructure of the hot-rolled water quenched samples. To determine the prior austenite grain size (PAGS) samples were etched in saturated aqueous picric acid at 68 °C and the PAGS was measured by the standard linear intercept method. The samples for SEM observations were etched with a 4% nital solution to reveal the overall microstructure, and subsequently analyzed using a Zeiss Ultra-55 field-emission scanning electron microscope running in a secondary electron mode.

For electron-backscattered diffraction (EBSD), the samples were vibration polishing with silica suspension. EBSD was

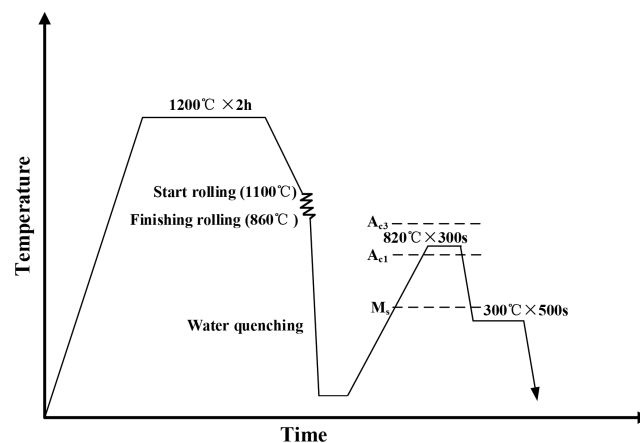


**Figure 1.** Schematics of the conditions of the hot rolling and Q&P heat-treatment processes used.

carried out at 20 kV with a step size of 0.09  $\mu\text{m}$ , and the HKL Channel 5 software was used for post processing.

To estimate the RA volume fractions and its average carbon content, X-ray diffraction (XRD) was carried out using a Bruker AXS D8-ADVANCE diffractometer equipped with a Cu  $K\alpha$  source, operating at 40 kV and 40 mA, in the  $2\theta$  range of 40–110° using a scanning step size of 0.01°. The volume fraction  $V_\gamma$  of RA in each steel sample was determined using the equation proposed by Cullity<sup>[23]</sup>

$$V_\gamma = \frac{1.4I_\gamma}{I_\alpha + 1.4I_\gamma} \quad (1)$$

where  $I_\gamma$  and  $I_\alpha$  are the average integral intensities of the (200), (220), and (311) face-centered cubic (FCC) peaks, and (200) and (211) body-centered cubic (BCC) peaks, respectively. The carbon content in the RA was estimated using the following equation<sup>[24]</sup>

$$\alpha_\gamma = 0.3556 + 0.00453x_c + 0.000095x_{Mn} \quad (2)$$

where  $\alpha_\gamma$  is the austenite lattice parameter, and  $x_c$  and  $x_{Mn}$  are the concentrations (wt%) of carbon and manganese, respectively.

#### 2.4. Determination of the Bainitic Transformation Behavior by Dilatometry

To determine the isothermal bainite formation behavior during the Q&P process for the three experimental steels, dilatometric experiments on the hot-rolled materials were performed. The dilatometry tests were carried out on a DIL 805 A D<sup>-1</sup> dilatometer using hot-rolled rectangular samples with dimensions of 2.5 × 4 × 10 mm<sup>3</sup>, keeping the longest axis of the specimen parallel to the plate rolling direction. The total volume fraction of bainite  $V_B$  was calculated from the dilatation curves using the lever rule method.<sup>[25]</sup> The change in the volume fraction of bainite was determined according to  $\Delta V_B = (\Delta l/l_{\max} \cdot V_B) \times 100\%$ , where  $\Delta l$  and  $l_{\max}$  are the change length caused by bainitic transformation and total length change caused by the completion of bainitic transformation, respectively. The heating, holding, and cooling process in the dilatometry test followed exactly the thermal profile of the Q&P process shown in Figure 1.

#### 2.5. Tensile Testing

The mechanical properties were analyzed using the tensile test samples (ASTM E8/E8M) with a gauge length of 25 mm and a width of 6 mm on a Shimadzu AG-X Plus 100 kN tensile testing machine with a crosshead displacement of 2 mm min<sup>-1</sup> at room temperature. To obtain the real stress–strain curve, an Omega extensometer was used. Data from three replicate samples of each steel grade were averaged. All measurements were carried out at room temperature.

The work-hardening behavior is related to the strain-induced transformation of RA to martensite. The instantaneous work hardening index  $n$  can be expressed as

$$n = d(\ln \sigma)/d(\ln \varepsilon) \quad (3)$$

where  $\sigma$  and  $\varepsilon$  are true stress and strain, respectively. Generally, good formability is characterized by a high  $n$  value.

### 3. Results

#### 3.1. Thermodynamic Calculation of Equilibrium Phase Fractions

Figure 2 shows the relationship between the holding temperature and the precipitated content of Nb (C, N) calculated using the Thermo-Calc software in combination with the TCFE9 database and the OM images of PAGS for the experimental steel slabs subjected to heating at 1200 °C for 2 h before final hot rolling and quenching. The thermodynamic results indicate that the temperature required for fully dissolving Nb (C, N) in the austenite matrix increases with increasing Nb content (Figure 2a). Specifically, this temperature is about 1200 °C for 0.027 wt% Nb steel B and 1300 °C for 0.061 wt% Nb steel C. The equilibrium volume fraction of the Nb (C, N) phase is even higher in the 0.061 wt% Nb steel C, resulting in the highest pinning force to reduce austenite grain growth. Indeed, the PAGS of steel C is smaller than that of steel A and B in Figure 2c,d. Nevertheless, it should be noted that the high temperature holding step used in this study may result in the coarsening of Nb (C, N) particles, which would reduce their ability to limit the austenite grain growth. When the quenched samples are reheated to 820 °C and held for 300 s during the Q&P process, the volume fraction of Nb (C, N) in steel C is much higher than that in steel B. Although this may be beneficial for grain refinement, as more carbon is consumed, the stability of the RA after the partitioning treatment may decrease.

#### 3.2. Microstructure Evolution

The OM images captured after the hot-rolled steels after quenching in water are shown in Figure 3. The microstructure is typically that of lath martensite. The austenite grains of steel B and steel C are more uniform in shape and size and are more refined in comparison with those of the Nb-free steel A, indicative of the well-known positive effect of Nb in grain size control.

The OM and SEM microstructures of the three test steels after Q&P treatment are shown in Figure 4. With increasing Nb content, the PAGS is effectively refined. The PAGS of steel A, steel B, and steel C is 8.7, 6.6, and 5.1  $\mu\text{m}$ , respectively. In the SEM images, the difference in final microstructure is not obvious as the prior austenite further is divided into different phases such as martensite, bainite, and ferrite. In addition to these microstructures, the final microstructure should also contain RA<sup>[5,26,27]</sup>; however, this is difficult to distinguish in the SEM images. Therefore, the distribution of RA is characterized and confirmed by EBSD and XRD.

The final microstructures after the Q&P process as analyzed by the EBSD data are shown in Figure 5. The white lines represent the low-angle boundaries in the range of 5–15°, and the black lines represent the high-angle boundaries above 15°. As shown in the band contrast maps and block sizes in Figure 5a–f, the microstructure is significantly refined when the Nb content increases. Figure 5g–i clearly shows the RA regions in green are surrounded by ferritic structures in red (i.e., bainite and martensite). Furthermore, there are some larger blocky RA grains in

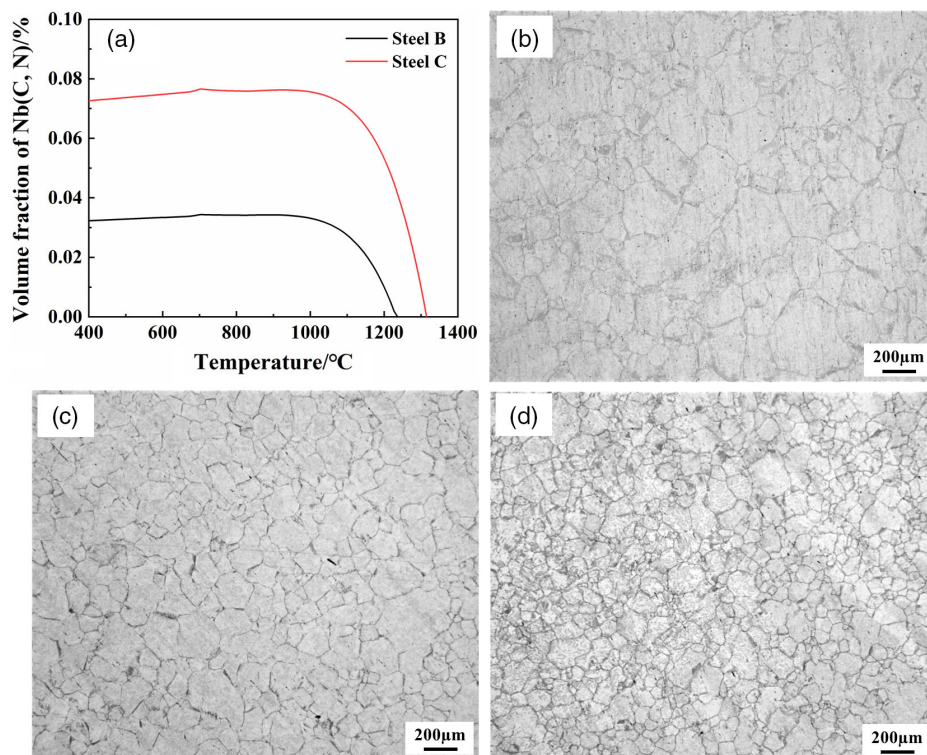


**Figure 2.** a) Equilibrium volume fractions of Nb (C, N) calculated by Thermal-Calc and OM images of PAGS for steels: b) steel A, c) steel B, and d) steel C.

Nb-free steel compared with Nb containing steels, but there is no significant difference in RA grain size between steel B and steel C from the RA grain frequency distribution of Figure 5j (results of multiple fields of view), the average grain size of RA for steel A, steel B, and steel C are  $0.48 \pm 0.12$ ,  $0.45 \pm 0.07$ , and  $0.44 \pm 0.06$   $\mu\text{m}$ , respectively. The spatial RA distribution becomes more uniform for the Nb containing steel grades.

Given the low volume fraction of RA in the EBSD phase maps in Figure 5, the volume fraction of RA cannot be measured accurately using this technique. Instead, the RA in the three experimental steels is examined by XRD. The XRD patterns and carbon contents of RA are shown in Figure 6. After the Q&P process, the diffraction peaks representing austenite in the three different steels are very similar, with only minimal differences. The volume fraction of RA remains approximately constant at  $9.70 \pm 0.24\%$  in all three steels. However, the corresponding carbon content in RA shows a monotonic decreasing trend, which influences the stability of RA to a certain degree. The error bars in Figure 6b reflect the uncertainty in the average carbon concentration related to the uncertainty in the determination of the exact location of the austenite diffraction peaks. The actual variation in carbon concentration between individual RA grains is of course much bigger.

### 3.3. Mechanical Properties

The aforementioned results revealed the (indirect) effects of Nb on the microstructure of the studied steels. Therefore, it could be assumed that Nb will also inevitably affect the mechanical

properties of the steel. The mechanical properties of the examined steels after the Q&P treatment are shown in Figure 7. The strength of the steel increases due to the addition of Nb. Steel B (0.027 wt% Nb) shows an increase in the YS and ultimate tensile strength (UTS) of  $\approx 40$  and 59 MPa with respect to the Nb-free steel A, whereas the total elongation (TEL) remains basically the same. As the Nb content is increased to 0.061 wt% (steel C), the YS and UTS increase by  $\approx 88$  and 144 MPa, respectively, but the TEL decreases by 2%. The strength–ductility results of the three investigated steels are shown in Figure 7c,d. Although the strength of steel C is significantly higher than those of steels A and B, its TEL is slightly lower. The strength–failure strain product of steel C is  $\approx 20.9$  GPa%, which is comparable with that of steel A without Nb. The product of strength–elongation of steel B is the highest at  $\approx 22.1$  GPa%.

To understand the work-hardening behavior of the studied steels, the tensile stress–strain curves were further analyzed. The  $n$  values of the steels are shown in Figure 7b. For steels A and B, the  $n$  values show a trend of monotonous decrease with increasing strain, whereas the  $n$  value of steel C increases slightly under low strain conditions, and then decreases significantly.

## 4. Discussion

### 4.1. Effect of the Nb Content on the Steel Microstructure

The grain growth of austenite can be effectively inhibited by the pinning effect of the Nb nanoprecipitate and the solution dragging effect of Nb. The precipitates provide a localized pinning

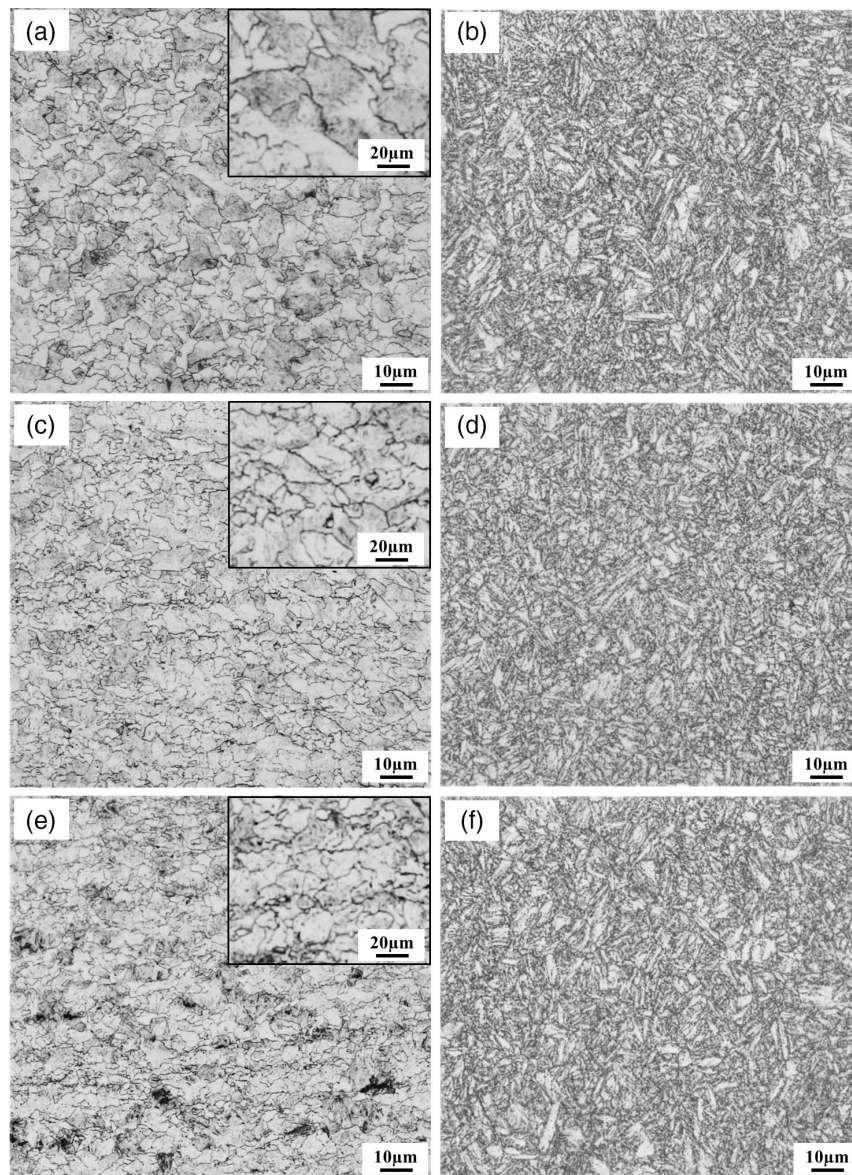


**Figure 3.** OM micrographs of prior austenite grains and microstructures of hot-rolled a,b) steel A, c,d) steel B, and e,f) steel C after quenching.

force at the grain boundary, whereas the slow diffusion of the Nb atoms segregated to the grain boundary provides a frictional resistance to the interface movement. Therefore, even when a small amount of Nb is added to the alloy, the microstructure of the hot-rolled steel is significantly refined (Figure 3). In addition, due to the inheritance of the prior microstructure during the Q&P the martensite and bainite lath are also refined, the formation of large blocky RA is significantly decreased and the density of highly misoriented grain boundaries is increased (Figure 5). These variations ultimately affect the mechanical properties of the experimental steel samples.

Several studies<sup>[28–32]</sup> have revealed that the bainitic transformation may occur during the partitioning step in Q&P steels. It has been suggested that pre-existing martensite affects the carbon enrichment of austenite and the nucleation number of bainite,

which can effectively improve the growth rate of the bainite and the bainitic transformation. Generally, the austenite grain boundary is the preferred nucleation position for bainite, as the energy barrier for grain boundary nucleation is significantly lower than that of internal nucleation; thus, the austenite grain size also affects the rate of bainitic formation. However, Hu et al.<sup>[32]</sup> reported that coarse austenite grains are beneficial for bainitic transformation. Although coarse austenite grains provide a smaller number of nucleation sites, the growth constraints of the bainite sheaves are decreased, resulting in an increased growth rate, and the second effect dominates over the nucleation density effect. This feature has also been reported by Xu et al.<sup>[33]</sup> **Figure 8** shows the bainite formation as a function of the holding time in the partitioning process for the three experimental steels. With increased Nb content, the volume fraction of bainite decreases gradually. The more rapid growth of bainite in

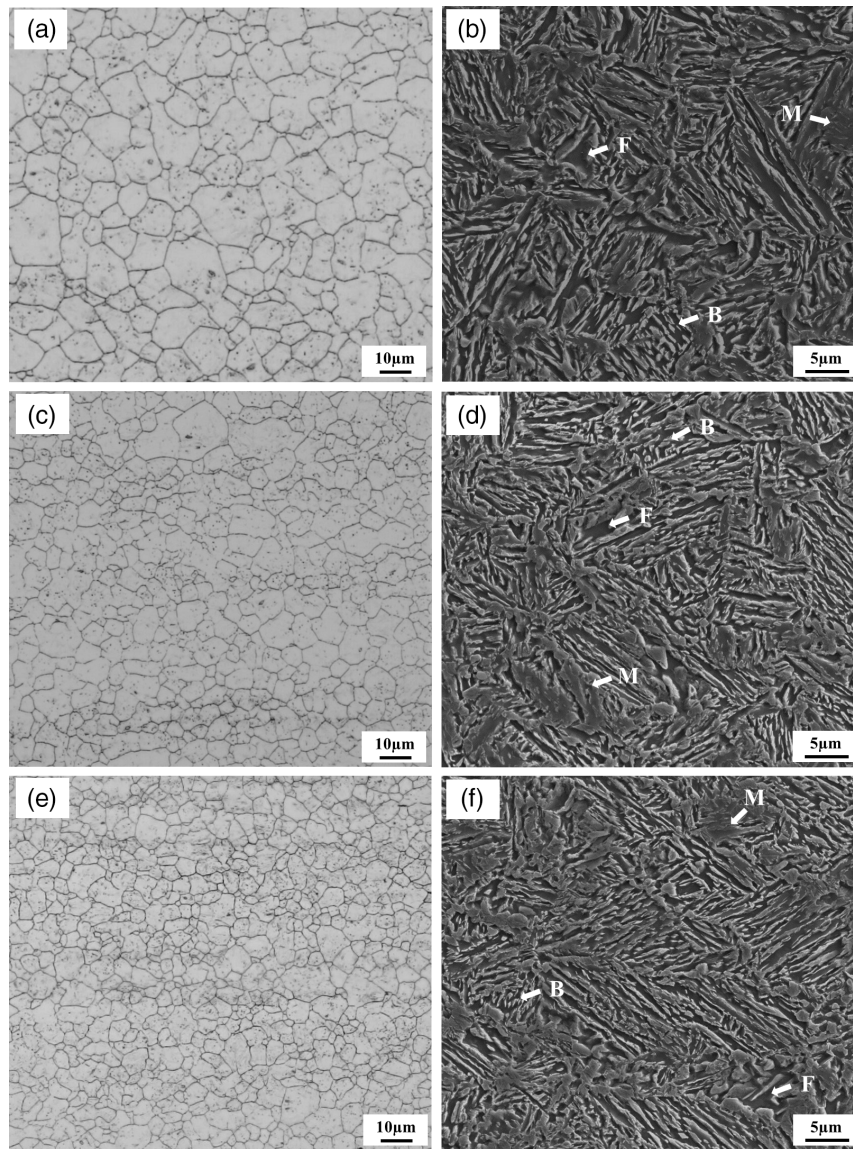


**Figure 4.** The OM and SEM images of the experimental steels after Q&P treatment: a,c,e) the PAGS of steels A, B, and C, respectively; b,d,f) the microstructures of steels A, B, and C, respectively.

the Nb-free steel with its larger grain size is due to fewer growth restrictions being present. As the Nb content reaches 0.061 wt%, the austenite grain size is smaller and the inhibition of the growth of bainite is greater.

Although Nb influences the volume fraction of bainite, a higher Nb content may not necessarily cause a decrease in the volume fraction of RA. According to Zhang et al.<sup>[10]</sup>, for Q&P steel containing Nb, due to the precipitation of Nb, carbon atoms are consumed, due to which the volume fraction of RA decreases for high Nb-containing steel. However, according to the results shown in Figure 6, as the Nb content increased, the volume fraction of RA did not change, which is a slightly different result from those of previous reports. It should be realized that the stability of the austenite grains during the Q&P process and hence the amount of RA at the end of the Q&P not only depends on the

RA chemistry (in particular its carbon content) but also on the morphology (size and shape) of the RA and the hardness and crystallographic orientation of its neighboring bainitic/martensitic matrix grains.<sup>[2,34]</sup> Therefore an increase in Nb leads to a reduction in the chemical stability, the microstructural refinement leads to an increase in physical stability, resulting in the RA fraction being more or less independent of the Nb content.

#### 4.2. Effect of the Nb Content on Mechanical Properties

As shown in Figure 7a, as the Nb content in the steels increase, the tensile strength increases significantly, whereas the corresponding elongation decreases for the highest Nb content. A major part of the strength increase is due to the grain size reduction, i.e., the Hall–Petch effect. In addition, as a water-cooling



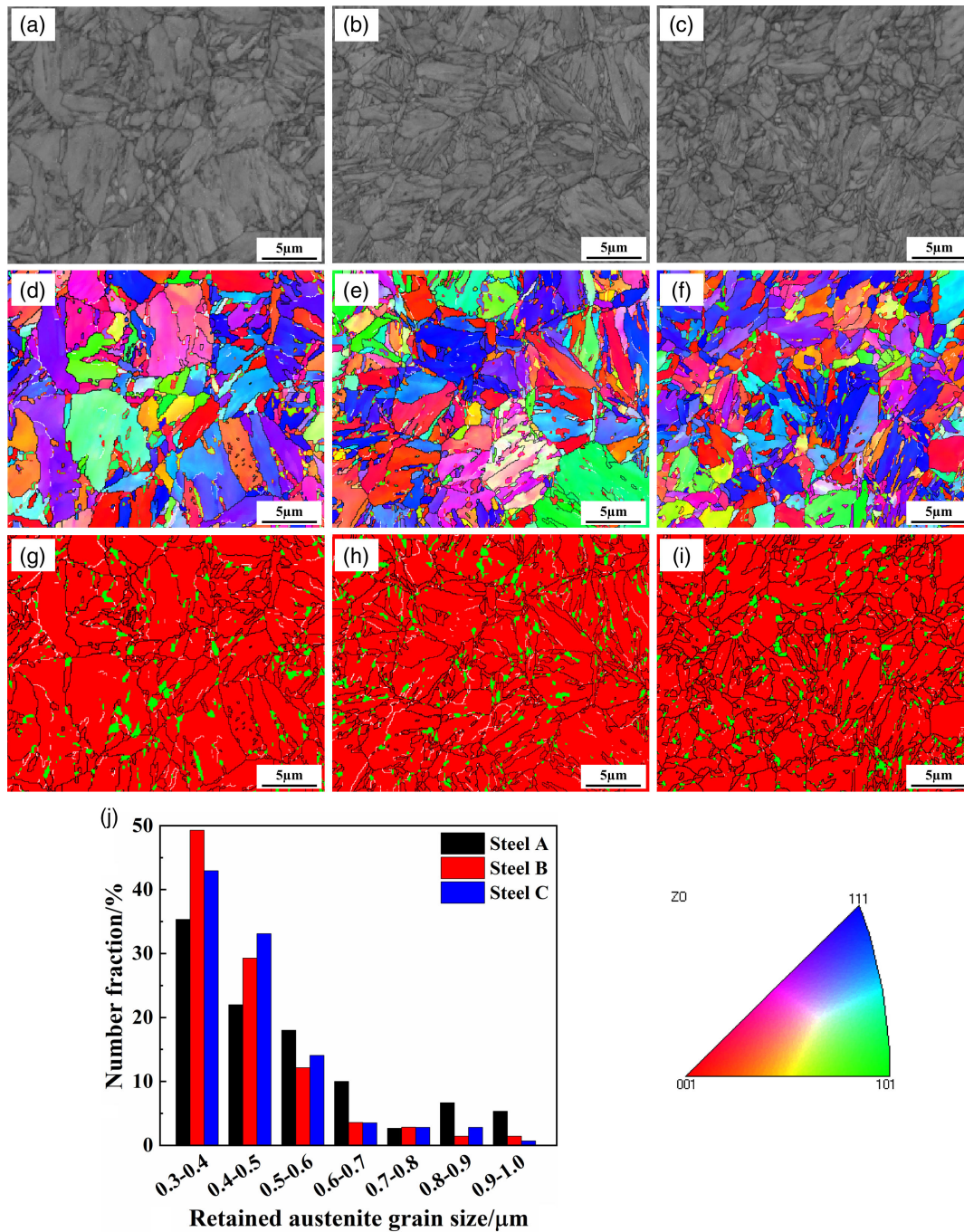


**Figure 5.** Crystallographic characteristics of investigated steels, obtained with EBSD: a–c) Band contrast maps of steels A, B, and C, respectively; d–f) Orientation images of steels A, B, and C, respectively; g–i) Morphological distribution of RA in steels A, B, and C, respectively, and j) RA grain frequency distribution of the three experimental steels.

strategy is used at the end of the hot-rolling process, some Nb might be retained in solid solution in the martensite matrix, which has the effect of solution strengthening. Moreover, according to the Orowan mechanism of precipitation strengthening, the precipitation of Nb (C, N) precipitates in the steel formed at higher temperatures also plays an important role in the strengthening, which also enhances the strengthening effect.

Its contribution to strength would be highest for steel C (0.061 wt% Nb) and although the volume fraction of bainite was lower than those of steels A and B, (the volume fraction of ferrite and tempered martensite being basically the same), its UTS remained the highest.

In addition to the passive strengthening mechanisms mentioned earlier, the transformation from austenite to martensite also plays

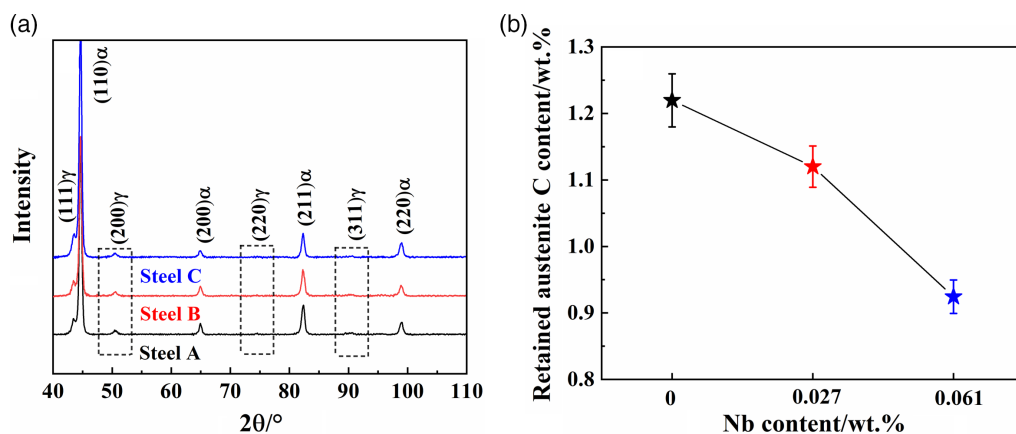


**Figure 6.** a) XRD patterns of the heat-treated samples; b) carbon content of RA. The scatter bars for the carbon concentration do only reflect the uncertainty in the average value due to the uncertainty in the location of the austenite diffraction peaks.

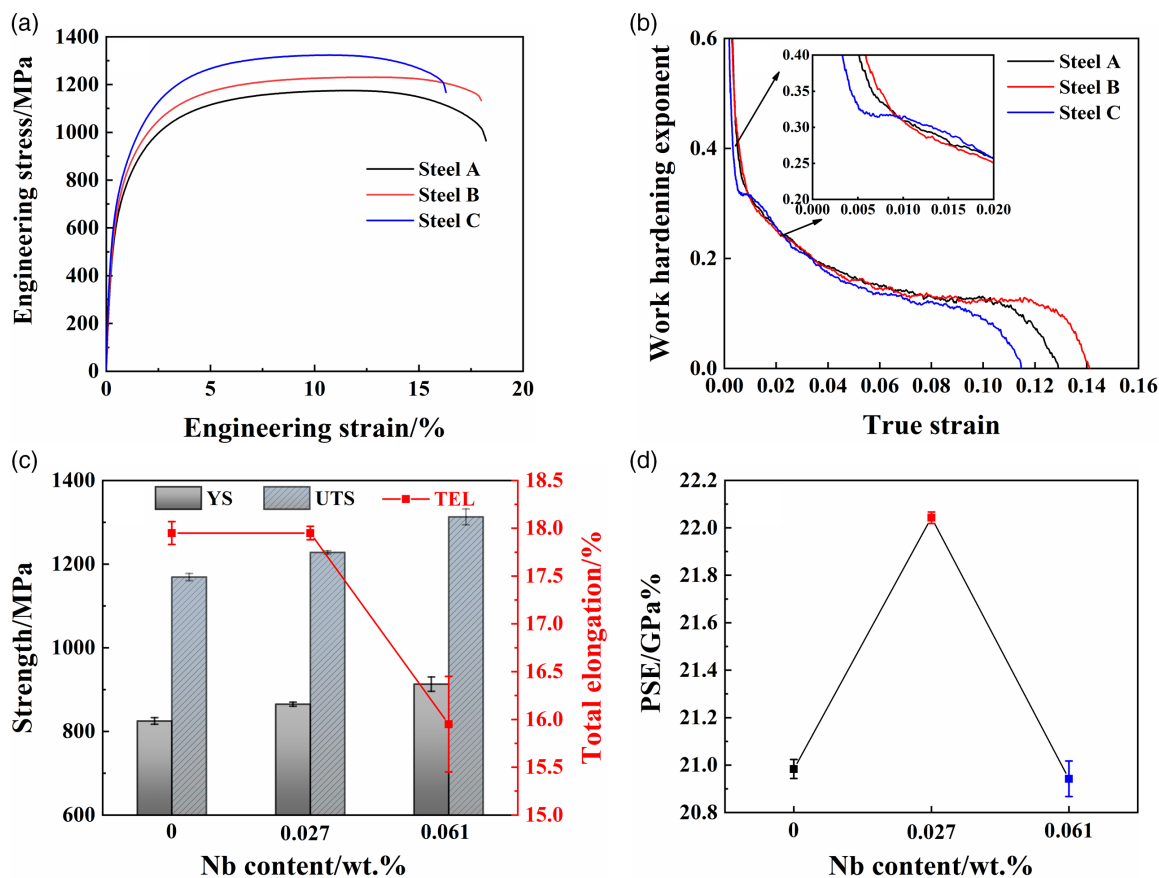


**Figure 7.** Mechanical properties of the experimental steels after the Q&P process: a) engineering stress–strain curves; b) instantaneous work hardening exponent–true strain curves; c) characteristic mechanical properties for the three steels; d) product of strength–elongation for the three steels.

an important role in the enhancement of the strength of steel. The unstable RA is more prone to the TRIP effect during the deformation, which enhances the strength and the strain hardening as a result of the formation of martensite with a high dislocation density.<sup>[10]</sup>

It is interesting to consider the strain-hardening behavior of the three steels with their equal volume fraction of RA but of

different chemical and physical stabilities. A first estimate of the effect of the reduced average carbon composition on the austenite stability can be obtained by calculating the  $M_s$  temperature using the average carbon concentrations, and assuming all other alloying element to be the nominal value (i.e., no substantial substitutional element partitioning). The results are shown in **Table 2**.

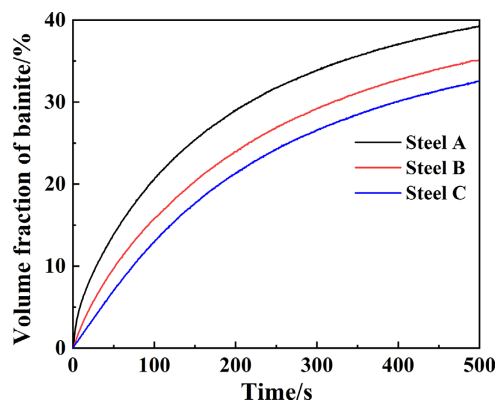


**Figure 8.** Bainite formation kinetics at 300 °C for 500 s.

**Table 2.**  $M_s$  temperature of steels having the same composition as the RA grains, according to JmatPro.

Steels	$M_s/^\circ\text{C}$
A	-53
B	18
C	56

The estimates based on the chemical composition only shows that the RA in steel A should be quite stable at room temperature and significant mechanical energy needs to be provided to induce the transformation. The RA in steel B is more or less stable at room temperature and little mechanical energy would be required to induce the transformation. Finally, the RA in steel C is predicted to be partially unstable at room temperature and it is only stabilized by its small grain size<sup>[35]</sup> and the mechanical constraints of the neighboring matrix.<sup>[36]</sup> In case we also consider that for very small RA grains the  $M_s$  temperature not only depends on its chemical composition but also on the grain size,<sup>[35]</sup> the predicted  $M_s$  temperatures are much lower and all are well below room temperature, i.e., the RA grains are stable at room temperature for all three steels, but their relative stability during mechanical deformation still varies in the manner, as shown in Table 2.

The differences in stability are nicely reflected in the strain-hardening curves. For Nb-free steel A, the work-hardening curve revealed a monotonous decrease in the work-hardening rate with increasing strain, and the work-hardening rate decreased slowly at higher strains. This result suggests that the TRIP effect occurred even though the RA had a high mechanical stability. The high carbon level in some RA may even result in the retention of a decent amount of RA that is not transformed into martensite upon completion of the tensile test. In the case of steel B, the work-hardening rate also decreases monotonically with strain. Compared with Nb-free steel A, the RA size of steel B is relatively smaller due to the fine grain effect of Nb, and the corresponding RA has higher mechanical stability. However, it has a lower chemical stability because of its lower carbon level. Ultimately, these results lead to the stability of RA being at a suitable level, and hence steel B exhibited the best work-hardening

behavior. In the case of steel C, the work-hardening curve rose slowly at low strain (Figure 7b), primarily due to the TRIP effect already occurring in the early stage of deformation (even during elastic deformation) of because of the chemical instability of the RA.<sup>[37–39]</sup> As the strain is increased, there is not enough RA fraction transforms into martensite in the middle and late stages of the deformation to further improve the work hardening ability, resulting in an abrupt decrease in the work-hardening rate and a reduction in elongation at break.

In summary, adding an appropriate amount of Nb into Q&P steel containing bainite can improve the strength, plasticity, and formability (work-hardening rate) of steel. However, at the highest Nb content the product of YS and tensile elongation decreased, which was attributed to the lower stability of the RA. Therefore, the optimal amount of Nb should be determined carefully to obtain the best strength–plasticity balance for low-carbon Q&P steels.

## 5. Conclusion

In this study, the effect of the Nb content on the final microstructure and mechanical properties of the Q&P steel contain bainite was investigated. The key findings are as follows: 1) The microalloying element, Nb, can significantly refine the microstructure of steel during Q&P treatment and delay the bainitic transformation in the partitioning stage. Moreover, as the Nb content in steel increases, the microstructure refinement and suppression of bainite transformation become more prominent. 2) Although Nb hardly affected the RA fraction of the studied steels, the carbon content in RA was reduced, resulting in a significant reduction in the stability of the RA. 3) Due to the microstructure refinement and the precipitation strengthening effects of Nb carbide, the tensile strength increased significantly with the increase in the Nb content. In addition, the TRIP effect could also contribute to the enhancement of strength under static tensile conditions. In particular, for the steel specimen with a high Nb content, the contribution to strength is relatively higher because of the poor mechanical stability of RA. 4) Due to the different stabilities of the RA in different Nb-containing steels, these samples exhibited different work-hardening behaviors at the same RA fraction. Further, an appropriate amount of Nb in steel leading to RA with a suitable carbon enrichment, a uniform spatial distribution, and a small grain size results in the best work-hardening ability.

## Acknowledgements

This work was supported by the National Natural Science Foundation of China (grant nos. U1808208, 51722101, and 52071066) and the Major Scientific and Technological Innovation Projects of Shandong Province (grant no. 2019TSLH0103). Dedicated to Prof. Wolfgang Bleck on occasion of his 70th birthday.

## Conflict of Interest

The authors declare no conflict of interest.

## Data Availability Statement

Research data are not shared.

## Keywords

bainitic transformation, Nb microalloying, quenching and partitioning steel, retained austenite, strength and total elongation

Received: April 27, 2021

Revised: July 17, 2021

Published online:

- 
- [1] W. Bleck, A. Frehn, E. Kechagias, J. Ohlert, K. Hulka, *Mater. Sci. Forum* **2003**, 426, 43.
- [2] C. Lesch, N. Kwiaton, F. B. Klose, *Steel Res. Int.* **2017**, *88*, 1700210.
- [3] Z. B. Dai, H. Chen, R. Ding, Q. Lu, C. Zhang, Z. G. Yang, S. van der Zwaag, *Mater. Sci. Eng. R* **2021**, *143*, 100590.
- [4] D. Frómeta, A. Lara, L. Grifé, T. Dieudonné, P. Dietsch, J. Rehrl, C. Suppan, D. Casellas, J. Calvo, *Metall. Mater. Trans. A* **2021**, *52*, 840.
- [5] J. Speer, D. K. Matlock, B. C. De Cooman, J. G. Schrothc, *Acta Mater.* **2003**, *51*, 2611.
- [6] F. H. Akbary, J. Sietsma, G. Miyamoto, T. Furuhashi, M. J. Santofimia, *Acta Mater.* **2016**, *104*, 72.
- [7] L. J. Zhao, L. H. Qian, J. Y. Meng, Q. Zhou, F. C. Zhang, *Scr. Mater.* **2016**, *112*, 96.
- [8] F. Peng, Y. B. Xu, J. Y. Li, X. L. Gu, X. Wang, *Mater. Des.* **2019**, *181*, 107921.
- [9] S. Chen, J. Hu, L. Y. Shan, C. C. Wang, X. M. Zhao, W. Xu, *Mater. Sci. Eng. A* **2021**, *803*, 140706.
- [10] J. Zhang, H. Ding, C. Wang, J. W. Zhao, T. Ding, *Mater. Sci. Eng. A* **2013**, *185*, 132.
- [11] E. D. Moor, J. G. Speer, D. K. Matlock, J. H. Kwak, S. B. Lee, *Steel Res. Int.* **2012**, *83*, 322.
- [12] E. D. Moor, J. G. Speer, D. K. Matlock, J. Penning, C. Fojer, *Mater. Sci. Technol.* **2009**, *3*, 1554.
- [13] G. Miyamoto, J. C. Oh, K. Hono, T. Furuhashi, T. Makic, *Acta Mater.* **2007**, *55*, 5027.
- [14] H. Y. Li, X. W. Lu, W. J. Li, X. J. Jin, *Metall. Mater. Trans. A* **2010**, *41*, 1284.
- [15] L. Samek, E. De Moor, J. Penning, B. C. De Cooman, *Metall. Mater. Trans. A* **2006**, *37*, 109.
- [16] X. C. Xiong, B. Chen, M. X. Huang, J. F. Wang, L. Wang, *Scr. Mater.* **2013**, *68*, 321.
- [17] D. Knijf, D. R. Petrov, C. Fojer, L. A. I. Kestens, *Mater. Sci. Eng. A* **2014**, *615*, 107.
- [18] H. Kong, Q. Chao, M. H. Cai, E. J. Pavlina, B. Rolfe, P. D. Hodgson, H. Beladi, *Metall. Mater. Trans. A* **2018**, *49*, 1509.
- [19] C. Klinkenberg, S. Trute, W. Bleck, *Steel Res. Int.* **2006**, *77*, 698.
- [20] S. H. M. Anijdan, S. Yue, *Mater. Sci. Eng. A* **2011**, *528*, 803.
- [21] L. J. Cuddy, *Metall. Trans. A* **1984**, *15*, 87.
- [22] N. Zhong, X. D. Wang, L. Wang, Y. H. Rong, *Mater. Sci. Eng. A* **2009**, *506*, 111.
- [23] B. D. Cullity, *Elements of X-Ray of Diffractions*, Addison-Wesley, Boston, MA **1978**.
- [24] N. H. van Dijk, A. M. Butt, L. Zhao, J. Sietsma, S. E. Offerman, J. P. Wright, S. van der Zwaag, *Acta Mater.* **2005**, *53*, 5439.
- [25] *ASTM International*, Designation: A 1033-10, **2015**.
- [26] D. V. Edmonds, K. He, F. C. Rizzo, B. C. De Cooman, D. K. Matlock, J. G. Speer, *Mater. Sci. Eng. A* **2006**, *438*, 25.
- [27] L. Wang, J. G. Speer, *Metall. Microstruct. Anal.* **2013**, *2*, 268.
- [28] S. Samanta, P. Bisis, S. Giri, S. B. Singh, S. Kundua, *Acta Mater.* **2016**, *105*, 390.
- [29] A. Navarro-López, J. Hidalgo, J. Sietsma, M. J. Santofimia, *Mater. Charact.* **2017**, *128*, 248.
- [30] D. Kim, J. G. Speer, B. Cooman, *Metall. Mater. Trans. A* **2011**, *42*, 1575.
- [31] S. Samanta, S. Das, D. Chakrabarti, I. Samajdar, S. B. Singh, A. Haldar, *Metall. Mater. Trans. A* **2013**, *44*, 5653.
- [32] F. Hu, P. D. Hodgson, K. M. Wu, *Mater. Lett.* **2014**, *122*, 240.
- [33] G. Xu, F. Liu, L. Wang, H. Hu, *Scr. Mater.* **2013**, *68*, 833.
- [34] D. D. Tjahjanto, A. S. J. Suiker, S. Turteltaub, P. E. J. Rivera Diaz del Castillo, S. van der Zwaag, *Comput. Mater. Sci.* **2007**, *41*, 107.
- [35] E. Jimenez-Melero, N. H. van Dijk, L. Zhao, J. Sietsma, S. E. Offerman, J. P. Wright, S. van der Zwaag, *Acta Mater.* **2007**, *55*, 6713.
- [36] B. B. He, M. X. Huang, A. H. W. Ngan, S. van der Zwaag, *Metall. Mater. Trans. A* **2014**, *45A*, 4875.
- [37] J. Hu, L. X. Du, Y. Dong, Q. W. Meng, R. D. K. Misra, *Mater. Charact.* **2019**, *152*, 35.
- [38] K. Hausmann, D. Krizan, K. Spiradek-Hahn, A. Pichler, E. Werner, *Mater. Sci. Eng. A* **2013**, *588*, 150.
- [39] Q. X. Feng, L. F. Li, W. Y. Yang, Z. Q. Sun, *Mater. Sci. Eng. A* **2014**, *603*, 175.